ARTICLES

Solubilization of Alkylcyanobiphenyl Liquid Crystals in Aqueous Micellar Solutions of a Diblock Copolymer of Propylene Oxide and Ethylene Oxide Studied Using Dynamic and Static Light Scattering

J. Fundin,[†] Z. Yang,[‡] A. Kelarakis,[§] I. W. Hamley,*[,†] C. Price,[‡] and C. Booth[‡]

Department of Chemistry, University of Leeds, Leeds LS2 9JT, U.K., Department of Chemistry, University of Manchester, Manchester M13 9PL, U.K., and Department of Chemistry, Physical Chemistry Laboratory, National and Kapodistrian University of Athens, Panepistimiopolis, 157 71 Athens, Greece

Received: November 29, 2001; In Final Form: August 29, 2002

The solubilization properties of $P_{60}E_{348}$ (P = oxypropylene, E = oxyethylene, subscripts = number of repeating units) diblock copolymer micelles containing liquid crystals have been studied by light scattering and UV spectroscopy for mainly dilute solutions from the following viewpoints: (i) the micellar solubilization rate J of a nematic liquid crystal (LC), predominantly pentylcyanobiphenyl, (ii) the amount of solubilized material at saturation, and (iii) the apparent size of the $P_{60}E_{348}$ micelles containing LC and their intermicellar interaction properties. It was shown, in experiments with solubilization temperature $T_s = 50$ °C, that the rate J is inversely proportional to the copolymer concentration c_p in the range 2 g $L^{-1} \leq c_p \leq 10$ g L^{-1} whereas J is constant at higher values of c_p. It was also shown that J increases strongly with an increase in temperature. The micellar hydrodynamic radius R_h was independent of temperature in the range 30 °C $\leq T \leq$ 60 °C, whereas there was a reduction in the hydrodynamic virial coefficient k_D and in the thermodynamic second virial coefficient A_2 as T was increased (for $T_s = 40$ °C). To probe the intermicellar interference, the excess scattered intensity was measured as a function of c_p, showing an increasing deviation from linearity, reflecting the transition from a dilute to a concentrated system and the increasing predominance of intermicellar interactions.

1. Introduction

The association behavior of amphiphilic block copolymers in selective solvents is attracting a great deal of industrial interest due to the increasing number of practical applications of these systems: in the colloidal dispersion technology of paints and coatings, home and personal care products, foams, oil additives, etc. Several reviews[1−8] and papers (for instance, see refs 9−13) carry extensive lists of references. Block copolymers can also be used as stabilizers to create nanostructured materials and nanoparticles, for extracting contaminated solids, or for drug delivery control.[14−19] The similarity of spherical block copolymer micelles to nanoscale biological systems and their transitions in shape opens a potential field for the development of models for biological cells.[20] Among the numerous applications resulting from their self-assembly in solution, solubilization is one of the most important ones.[21−23] In the case of water-based systems, the core provides an appropriate microenvironment for hydrophobic molecules that are incompatible with the solvent. Solubilization is a phenomenon that is the basis from which many practical applications of surface active agents are derived. Suitable block copolymer micelles in water exhibit selective solubilization of aromatic hydrocarbons compared to aliphatic hydrocarbons, and this has been exploited for applications in drug delivery and flavor/fragrance release systems.[6] Hurter and Hatton[22] reported that the solubilization, which we from now on are going to refer to as the saturation solubility c_s (see ref 24), by micelles of block copolymers with oxyethylene and oxypropylene blocks depends strongly on the molecular architectures of the micelle-forming copolymers where linear triblock copolymers are more accommodating than branched tetronic copolymers, which is due to the ability of the former to self-assemble into more compact micelles.[22] It is believed that steric effects attributed to branched copolymers result in looser micellar aggregates, which would imply a less apolar environment in the core compared to that in micelles of linear block copolymers. Gadelle et al.[25] emphasize that c_s of aromatics is highly dependent on the copolymer structure in terms of P and E unit numbers, P/E ratio and molecular weight of the copolymer. Also, their results show that under certain circumstances, solutions of triblock copolymers of P and E units can be better solubilizers than those of standard low-molecular weight surfactants.

Although block copolymer micelles are widely used to accommodate aromatic molecules, they have yet to be exploited to accommodate LCs. To our knowledge, such properties have never been investigated before with the exception of a recent study on solutions of $P_{94}E_{316}$ containing LC carried out in our

* Corresponding author. Phone: +44 (0)113 343 6430. Fax: +44 (0)-113 343 6565. E-mail: I.W.Hamley@chem.leeds.ac.uk.
[†] University of Leeds.
[‡] University of Manchester.
[§] National and Kapodistrian University of Athens.

10.1021/jp014356o CCC: $22.00
Published on Web 10/23/2002

laboratories;[26] a block copolymer of higher hydrophobicity (P/(P + E) mole ratio $r = 23\%$) than the one described in the present paper ($r = 15\%$). Diblock copolymers were chosen because it has been shown that diblocks form micelles at lower concentrations and at lower temperatures than triblocks, and the former are therefore better solubilizers.[12] Among the more important observations it was concluded that the solubilization process of LC in $P_{94}E_{316}$ micelles is thermally reversible. Investigation of the solubilization of nematic LC in block copolymer micelles could be important to future applications within the display technology industry. The work is also of fundamental interest due to the effect on LC phase behavior of confinement in a spherical geometry. This can lead to the suppression of the nematic−isotropic phase transition temperature[27] or to surface-induced orientational order.[28] Fundamental work on confinement of LC within micelles should lead to new insights into the effect of reduced dimensionality on LC phase behavior. One may hope to exploit this property to prepare nanoscale patterned LC domains on a solid substrate, specifically hexagonal domain structures self-assembled from block copolymers spin coated in thin films with LC selectively solubilized within the hexagonal nanostructure. Numerous applications have already been envisaged for thin block copolymer films on the basis of a hexagonal domain structure, such as filters or in high-density data storage media.[6,29] Here, as a further step toward novel applications, we investigate the solubilization of a nematic liquid crystal in a micellar solution of the diblock copolymer $P_{60}E_{348}$.

2. Experimental Section

2.1. Polymer Preparation and Characterization. The polymer $P_{60}E_{348}$ was prepared by sequential anionic polymerization of propylene oxide (P) followed by ethylene oxide (E). The preparation and characterization methods employed were similar to those described in detail elsewhere.[12,30] To remove moisture, ampule and vacuum line techniques were used. The monofunctional initiator, 1-methoxy-2-propanol was activated by reaction with potassium metal (mole ratio OH/K $\approx$ 9). The precursor poly(oxypropylene) and the final PE diblock copolymer were sampled, followed by characterization of the two samples by gel permeation chromatography (GPC) (eluent: *N*,*N*-dimethylacetamide, $T = 60$ °C) calibrated with poly(oxyethylene) standards to define the width of their chain length distributions, i.e., M_w/M_n, where M_w and M_n are the weight- and number-average molecular weights, respectively. To account for instrumental spreading in the system, a small correction to the quantity M_w/M_n was made. It was shown that the impurity content was about 2% (w/w), concluded to be due to the presence of triblock copolymer, indicated by a minor shoulder on the low elution volume side of the GPC peak of the copolymer. Analysis of ^{13}C NMR spectroscopy measurements was based on the assignments by Heatley et al.[31] Absolute values of M_n and the overall composition (mole percent of E units) were obtained from comparison of integrals from end-group and backbone carbons. A minor quantity, 0.3 mol %, of unsaturated ends originating from the transfer reaction in the anionic polymerization of propylene oxide[32] was included in the calculation. The formula of the copolymer $P_{60}E_{348}$ was accurately determined from M_n of the precursor P block and the overall composition. $M_n = 18\ 800$ and $M_w/M_n = 1.08$.

2.2. Sample Preparation for Light Scattering. Three gram quantities of aqueous solutions of the $P_{60}E_{348}$ diblock copolymer in the concentration range 2 g $L^{-1} \le c_p \le 36$ g L^{-1} were obtained by dilution of a concentrated stock solution with Milli-Q-grade water. Two drops of nematic LC were added with a Pasteur pipet. The liquid crystal mixture used was Licrilite BL002, from Merck, U.K., pentylcyanobiphenyl 40−60%, nematic temperature range -20 °C $\le T \le 80$ °C. The product contains oxyalkyl substituents as well as alkyl. This addition of LC was in large excess compared with amount solubilized. The samples were stirred for approximately 16 h at solubilization temperatures T_s of 40 and 50 °C, whereafter they were quickly filtered into 10-mm diameter light scattering cells through 0.20-μm Millex-GN nylon membrane filters from Millipore. Experiments were carried out with 5 °C $\le T \le 60$ °C.

2.3. Dynamic and Static Light Scattering (DLS and SLS). The techniques and their applicability to colloidal solutions are described in detail elsewhere.[12,30,33,34] DLS measurements were made by means of a Brookhaven BI 9000 AT digital correlator combined with a Malvern PCS100 instrument with vertically polarized incident light of wavelength $\lambda = 488$ nm supplied by a Coherent Innova 90 argon-ion laser operating at 500 mW or less. Measurements of the scattered light were usually made at the detector angle $\theta = 90°$ to the incident beam. The time-dependent intensity correlation function of the radiated light $g_2(t)$ is related to the electric field correlation function $g_1(t)$ according to the Siegert relation:

$$g_2(t) = B(1 + \beta|g_1(t)|^2) \tag{1}$$

where B is a baseline and β is a factor that takes into account deviations from ideal correlation. For a continuous distribution of relaxation rates, inverse Laplace transformation (ILT) can be used:

$$g_1(t) = \int_0^\infty G(\Gamma) \exp(-\Gamma t)\, d\Gamma \tag{2}$$

where $G(\Gamma)$ is the decay rate distribution, which was obtained from analysis of the DLS correlation functions using CONTIN.[35] Translational diffusion coefficients D were calculated from the ILT moments as $D = \Gamma/q^2$, where q is the scattering vector qiven by $q = (4\pi n/\lambda)\sin(\theta/2)$. Here, n is the refractive index of the scattering medium and θ is the scattering angle, defined as the angle between the wave vector of the electric field of the incident radiation $\vec{k}_0$ and the wave vector of the scattered field $\vec{k}_s$ that reaches the detector. The concentration dependence of D is usually expressed as

$$D = D_0(1 + k_D c) \tag{3}$$

where D_0 is the diffusion coefficient at infinite dilution, c is the concentration of the solute, and k_D (ref 36) is referred to as the hydrodynamic virial coefficient because it is in part related to the hydrodynamic interactions in the solution by

$$k_D = 2A_2M_w - k_f - 2\upsilon_2 \tag{4}$$

Here, A_2 is the thermodynamic second virial coefficient, k_f describes the concentration dependence of the friction factor f, and υ_2 is the partial specific volume of the solute (in this case the block copolymer−LC complex). The hydrodynamic radius R_h can be obtained from the Stokes−Einstein equation:

$$R_h = \frac{k_B T}{6\pi\eta_0 D_0} \tag{5}$$

where k_B is the Boltzmann constant and η_0 is the viscosity of the pure solvent at temperature T. (The apparent hydrodynamic

radius $R_{h,app}$ is given by a similar expression where D_0 in (5) is replaced by D, i.e., at $c > 0$.)

SLS measurements were done under similar conditions using the same Malvern instrument described above. The basis for analysis of the integrated intensities was the Rayleigh−Gans−Debye equation:

$$S - S_0 = Kc_pM_w \tag{6}$$

S is the intensity of light scattered from solution relative to that from benzene, S_0 is the corresponding quantity for the solvent, c_p is the polymer concentration in units g L^{-1}, and K is the optical constant given by

$$K = \left(\frac{4\pi^2}{N_A\lambda^4}\right)\left(\frac{n_B^2}{R_B}\right)\left(\frac{dn}{dc}\right)^2 \tag{7}$$

where N_A is Avogadro's constant, n_B and R_B are the refractive index and Rayleigh ratio of benzene, respectively, and dn/dc is the specific refractive index increment of the solute in a given solvent. Values of dn/dc, its temperature dependence, and other quantities necessary for the calculations have been given elsewhere for block copolymers in the absence of LC.[30] Values of dn/dc are very similar for E and P, and are therefore insensitive to the exact compostion of the copolymers, and correction for refractive index difference within the copolymers is not necessary. Values of dn/dc were not measured at saturation solubility, so values of M_w from SLS of micelles + LC are apparent.

2.4. Solubilization Rate Measurements. The samples were thermostated at 21 °C for approximately 24 h, whereafter the excess scattered light intensity was detected as a function of time at the fixed temperatures 50 and 60 °C, which are above the critical micellization temperature (cmt).

2.5. Saturation Solubility c_s. The sample preparation was the same as that for light scattering (see above). For the measurements a Hewlett-Packard 8452 UV/vis spectrometer was used. It was calibrated by recording the absorbances of methanol solutions of LC in the concentration range 4 mg $L^{-1} \le c \le 40$ mg L^{-1} and in the wavelength interval 190 nm $\le \lambda \le$ 400 nm compared to a solvent reference. Dilution with water was not possible, because that led to dissociation of the micelles and precipitation of the LC. The strong absorbance at $\lambda = 288$ nm was found to follow the Lambert−Beer law. The dilutions used in the experiments resulted in solutions containing no more than 0.5% (w/w) water, and the calibration for methanol solutions was used without correction.

2.6. Critical Micelle Concentration (cmc) by Surface Tension. The cmc values for $P_{60}E_{348}$ in water at 30 °C (2.3 g L^{-1}) and 40 °C (0.29 g L^{-1}) were measured by employing the Du Noüy ring method. The surface tension γ was measured as a function of the concentration by using an automatic processor tensiometer from Krüss (model K12), which provides a temperature-controlled environment (±0.1 deg). Automatic sequential dilution of stock solutions of $P_{60}E_{348}$ in Milli-Q-grade water were made using a Metrohm 765 Dosimat connected to the tensiometer. The cmc values fitted the van't Hoff equation ($d \ln K/d(1/T) = -\Delta_r H°/R$, where $\Delta_r H°$ is the standard reaction enthalpy at the temperature T, and R is the gas constant) established by cmc values measured in the range 18−26 °C using light scattering and dye solubilization.[37] Extrapolation gave cmc = 0.023 g L^{-1} at 50 °C and 0.003 g L^{-1} at 60 °C. Thus, all results presented in this report are attributed to the micellar region, well above the cmc.

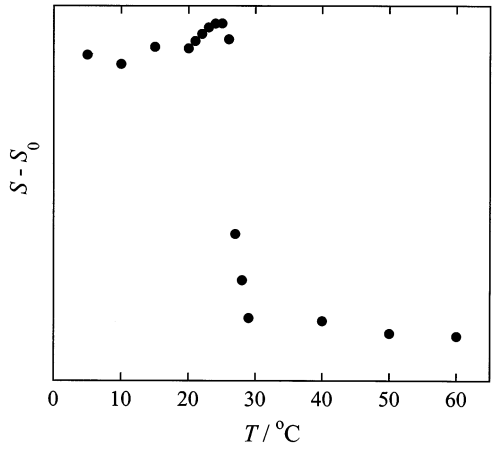

Figure 1. Scattering function $S - S_0$ vs temperature T, for 20 g L^{-1} $P_{60}E_{348}$ + LC, and for $T_s = 40$ °C.

3. Results and Discussion

3.1. Solubilization and the cmt. Figure 1 shows the scattering function $S - S_0$, on an arbitrary scale, plotted against temperature for a 20 g L^{-1} solution of $P_{60}E_{348}$ containing LC solubilized at $T_s = 40$ °C. T was increased in steps from 5 to 60 °C, and at each step, $S - S_0$ was registered after waiting a few minutes. The result is similar to that reported by Yang et al.[26] for the copolymer $P_{94}E_{316}$. Recent work has shown that the cmt of a 20 g L^{-1} solution of $P_{60}E_{348}$ is 20 °C,[37] and the data in Figure 1 are consistent with this as no micelles are present at $T < 20$ °C, implying a macroscopic phase separation between the nematic mesophase (LC) and the isotropic liquid phase (molecular $P_{60}E_{348}$ + water). The resulting turbid colloidal dispersion present at 5 °C $\le T <$ 20 °C gives a high scattered intensity. Above $T = 20$ °C, micelles are formed and the excess intensity increases. After a time, at which point the temperature has reached 26 °C, the solubilization of LC becomes the overriding factor that leads to a reduction in $S - S_0$ and eventually an optically clear solution. It should be noted that the values of $S - S_0$ in the narrow interval 26 °C $\le T \le$ 30 °C are registered out of equilibrium; i.e., at a time before the saturation solubility c_s is reached. An objective of this set of measurements was confirmation of the cmt, and for that purpose we did not need the equilibrium values of $S - S_0$, which may take several hours to reach at low temperatures. However, at 40 °C $\le T \le$ 60 °C, the solubilization rate J is relatively fast, and equilibrium values of $S - S_0$ were obtained after a few minutes. (See below for a discussion of rate measurements.) The results depicted are representative for the present system under a variety of conditions.

3.2. Particle Size by DLS. Parts a and b of Figure 2 show distributions of $R_{h,app}$ in the temperature interval 5−60 °C, for 20 g L^{-1} $P_{60}E_{348}$ diblock copolymer with the LC solubilized at $T_s = 40$ °C. As noted above, cmt ≈ 20 °C, which implies that the major peak observed in the distributions in Figure 2a is attributable to LC droplets. The width of the LC peak indicates a wide distribution of droplet size. At 25 °C the cmt was exceeded, which is indicated by the appearance of a small peak attributable to micelles. As temperature was increased in the interval 30−40 °C (see Figure 2b) the micelle peak increased in intensity at the expense of the LC peak. The LC peak was always present at $T \le T_s$. At $T > T_s$ only the micelle peak was present, as all LC was solubilized.

The temperature dependence of $R_{h,app}$ is shown in Figure 3. The increase in $R_{h,app}$ of the LC droplets, from about 55 to 150 nm, presumably results from transfer of copolymer surfactant

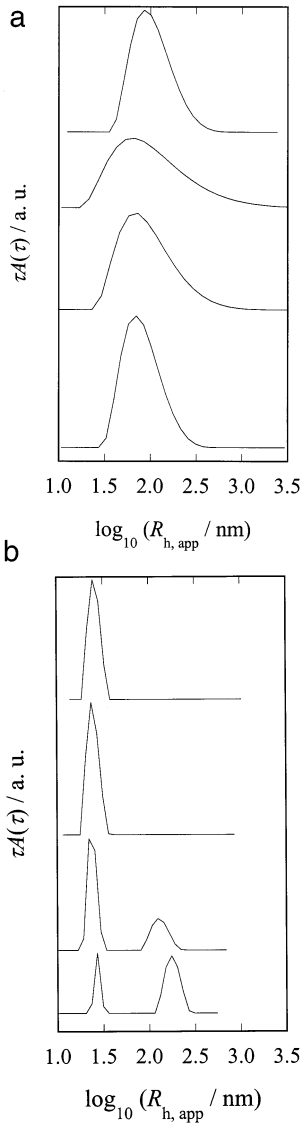

Figure 2. Distributions of $R_{h,app}$ for 20 g L^{-1} $P_{60}E_{348}$, and for $T_s = 40$ °C. Temperatures (from the bottom): (a) 5, 10, 15, and 20 °C; (b) 30, 40, 50, and 60 °C.

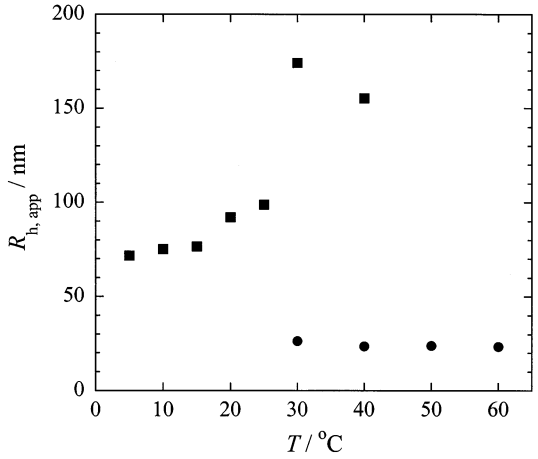

Figure 3. Temperature dependence of $R_{h,app}$ for block copolymer micelles (●) and for free LC droplets (■) in a solution of 20 g L^{-1} $P_{60}E_{348}$. $T_s = 40$ °C.

from droplet surface to micelles as the extent of micellization increases with increasing T.[37] A reduction in the proportion of copolymer available to stabilize the surface of the droplets will force an increase in droplet size. The micelle radius, on the other hand, is independent of T ($T \geq 30$ °C) which agrees with other reports in the literature about block copolymer micelles.[38,39] $R_{h,app}$ is constant at about 25 nm. The temperature independence of $R_{h,app}$ is a result of the interplay of two effects. As T is increased, the micelle aggregation number increases, but simultaneously the swelling of the micelle E-block corona decreases, and the two effects cancel each other out. All parameters determined by dynamic and static light scattering are given in Table 1.

TABLE 1: DLS and SLS Parameters of Micellar $P_{60}E_{348}$ with Solubilized LC

T_s/ °C	T/ °C	R_h/ nm	$10^{-5}M_{w,app}$/ g mol^{-1}	δ_t	r_t/ nm	10^5A_2/ mol mL g^{-2}	10^3k_D/ L g^{-1}
40	50	27	42	9.0	25	0.9	5.9
40	60	27	47	8.9	26	0.8	2.9
50	50	23	24	6.5	19	1.2	2.3
50	50	74[a]					−21.6[a]
50	60	29	40	9.5	25	1.0	6.5

[a] Apparent parameters of LC droplets. $A_2 = 4N_{A}v_t/M^2$ (see text for definitions).

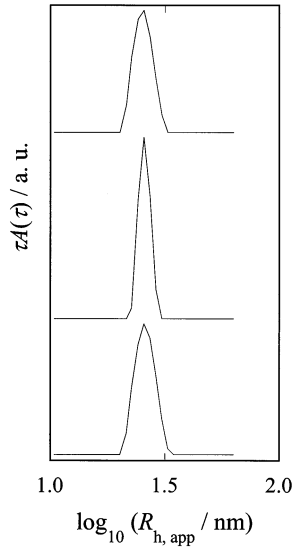

Figure 4. Distributions of $R_{h,app}$ for $P_{60}E_{348}$ + LC at $T_s = 40$ °C and $T = 50$ °C. Concentrations of $P_{60}E_{348}$ (from the bottom): 10, 16, and 26 g L^{-1}.

3.3. Micelle Mass and Expansion Factor by SLS. Considering the results in section 3.2, it can be deduced that a solution which is essentially completely micellar and which is studied at a temperature higher than that at which the LC was solubilized (i.e., $T > T_s$) should give light scattering data that are not complicated by the presence of LC droplets. The DLS results presented in Figure 4 for solutions of $P_{60}E_{348}$ equilibrated with LC at $T_s = 40$ °C then filtered and studied at $T = 50$ °C confirm that this is so for solutions of concentration $c_p > 10$ g L^{-1}. Inverse Laplace transformation (ILT) of time-dependent autocorrelation functions showed single-exponential decays, corresponding to unimodal distributions of apparent hydrodynamic radii, where the peak amplitude for each experiment was equal to that of the moments of the autocorrelation function for the entire solution. The peak position corresponds to the size of the block copolymer micelles saturated with LC. On saturation, a transition from spherical to cylindrical shape might occur if the E-block lengths are short.[40] Expansion of the core increases the surface area, and surface coverage can become insufficient to stabilize the micelle. The sphere-to-cylinder transition reduces

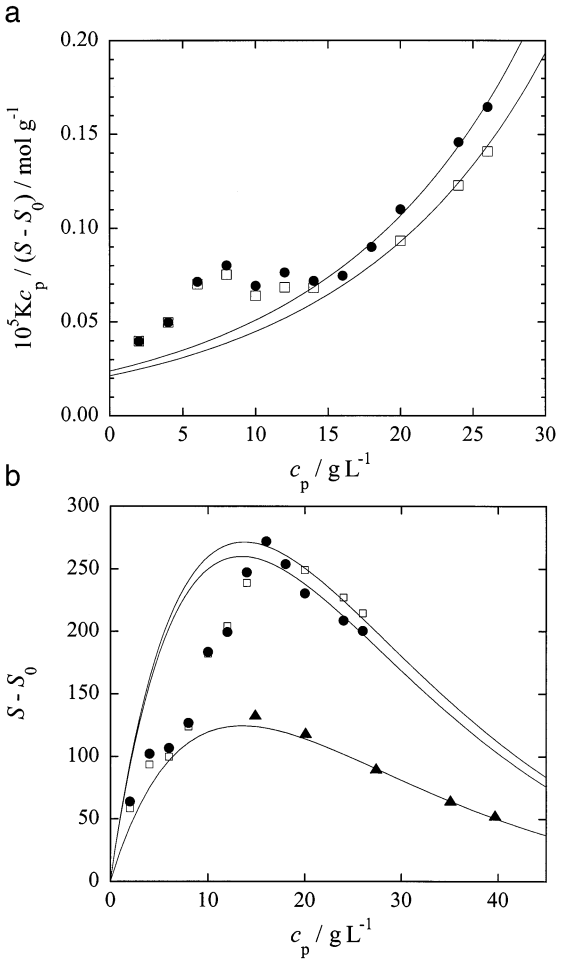

Figure 5. (a) Debye plots for $P_{60}E_{348}$ + LC at $T = 50$ (●) and 60 °C (□). $T_s = 40$ °C. (b) Integrated excess intensity $S - S_0$ vs concentration of $P_{60}E_{348}$ at $T = 50$ (●) and 60 °C (□) and for $T_s = 40$ °C. For comparison, data for $P_{60}E_{348}$ in the absence of LC at $T = 50$ °C (▲) are included.

the surface-to-volume ratio. However, in our case where the E-block length is very long, the transition is most unlikely. Furthermore, from small-angle X-ray scattering measurements on similar PE diblock copolymer micelles saturated with LC there is evidence of a spherical micellar shape.[41] Similar unimodal distributions were found for the same solutions at $T = 60$ °C.

Figure 5a shows Debye plots for solutions containing LC solubilized at 40 °C then filtered and investigated at 50 and 60 °C. The mass ratio c_p/c_{LC} is assumed to be the same for the two sets of data. Curvature arises because of inceased interference between scattering centers as concentration is increased. If the micelles are modeled as uniform hard spheres, the Perkus−Yevick theory can be applied in the form suggested by Vrij[42] and incorporating the Carnahan−Starling equation,[43] that is

$$\frac{Kc_p}{S - S_0} = \frac{1}{M_w Q} \tag{8}$$

where the structure factor Q is defined by

$$1/Q = [(1 + 2\phi)^2 - \phi^2(4\phi - \phi^2)](1 - \phi)^{-4} \tag{9}$$

ϕ is the volume fraction of equivalent hard spheres determined from the volume of an anhydrous micelle by applying a

TABLE 2: Mass of Solubilized LC in Micelles of $P_{60}E_{348}$

c_p/ g L^{-1}	T/ °C	c_s/mg of LC per g of copolymer
10	40	20
10	50	24
20	40	26
20	50	31
30	40	26
30	50	30

thermodynamic expansion factor δ_t, defined as

$$\delta_t = \nu_t/\nu_a \tag{10}$$

where ν_t is the thermodynamic volume (one-eighth of the excluded volume) of a micelle and ν_a is the anhydrous volume, which in turn is given by $\nu_a = M_w/N_A\rho_a$, where N_A is Avogadro's constant and ρ_a the density of the dry copolymer. The parameter ρ_a was calculated from the known specific volumes of the homopolymers at the appropriate temperature.[44]

The experimental results are compared with theory in Figure 5a. The value of dn/dc used in the calculation was that for copolymer $P_{60}E_{348}$ alone in solution, and the derived values of M_w (but not those of δ_t) are somewhat incorrect on that account. As for solutions of the copolymer alone,[37] it was not possible to fit the data across the full range of concentration. In fact, as illustrated, fits were possible only at high values of c_p. The parameters used to fit the two sets of data, i.e., apparent values of M_w and true values of δ_t, are listed in Table 1. In the experiment the block copolymer (CP) molecules exist as molecules in solution, or are in micelles, or are adsorbed on droplet surfaces. At low c_p a larger proportion of the CP molecules stabilize the droplets, and so there are fewer micelles. Moreover, because the molecules are involved in two equilibria (micellization and adsorption) the concentration of free molecules is doubly lowered. When the droplets are removed by filtration, so is the adsorbed copolymer, and the CP solution is more dilute than that expected from the preparation. An upturn in $Kc_p/S - S_0$ would occur because of this.

The effect of intermicellar interference can be seen more clearly if $S - S_0$ is plotted against c_p, as in Figure 5b. In this case a maximum in the scattering curve arises because of increased interference between scattering centers as concentration is increased. For comparison, data points taken from ref 37 for copolymer $P_{60}E_{348}$ at 50 °C without LC are included in the figure. In that case scattering from dilute solutions was not investigated. As reported in ref 37, the fit to these points corresponds to $M_w = 2.0 \times 10^6$ g mol^{-1} and $\delta_t = 10.4$. Although only apparent values were obtained for the systems containing LC, the larger molar masses of those micelles are consistent with solubilization of the LC. The unchanged expansion factor of the E-block corona is consistent with solubilization solely within the P-block core. The solid curves are fits according to the Carnahan−Starling equation mentioned above (eqs 8 and 9) where the excluded-volume interaction is taken into account. As reported in Table 2, as determined by UV spectroscopy, the amount of solubilized LC relative to copolymer was 2.5 ± 0.5% (w/w). However, the apparent molecular weight reported in Table 1 for micelles of copolymer plus LC at 50 °C (approximately 4×10^6 g mol^{-1}) is double that reported for the copolymer alone ($M_w = 2 \times 10^6$ g mol^{-1}).[37] Because the amount of LC solubilized is relatively small compared to copolymer, it is unlikely that this can be attributed entirely to an increase in dn/dc. Accordingly, we conclude that solubilization of the LC leads to a significant increase in aggregation number of the

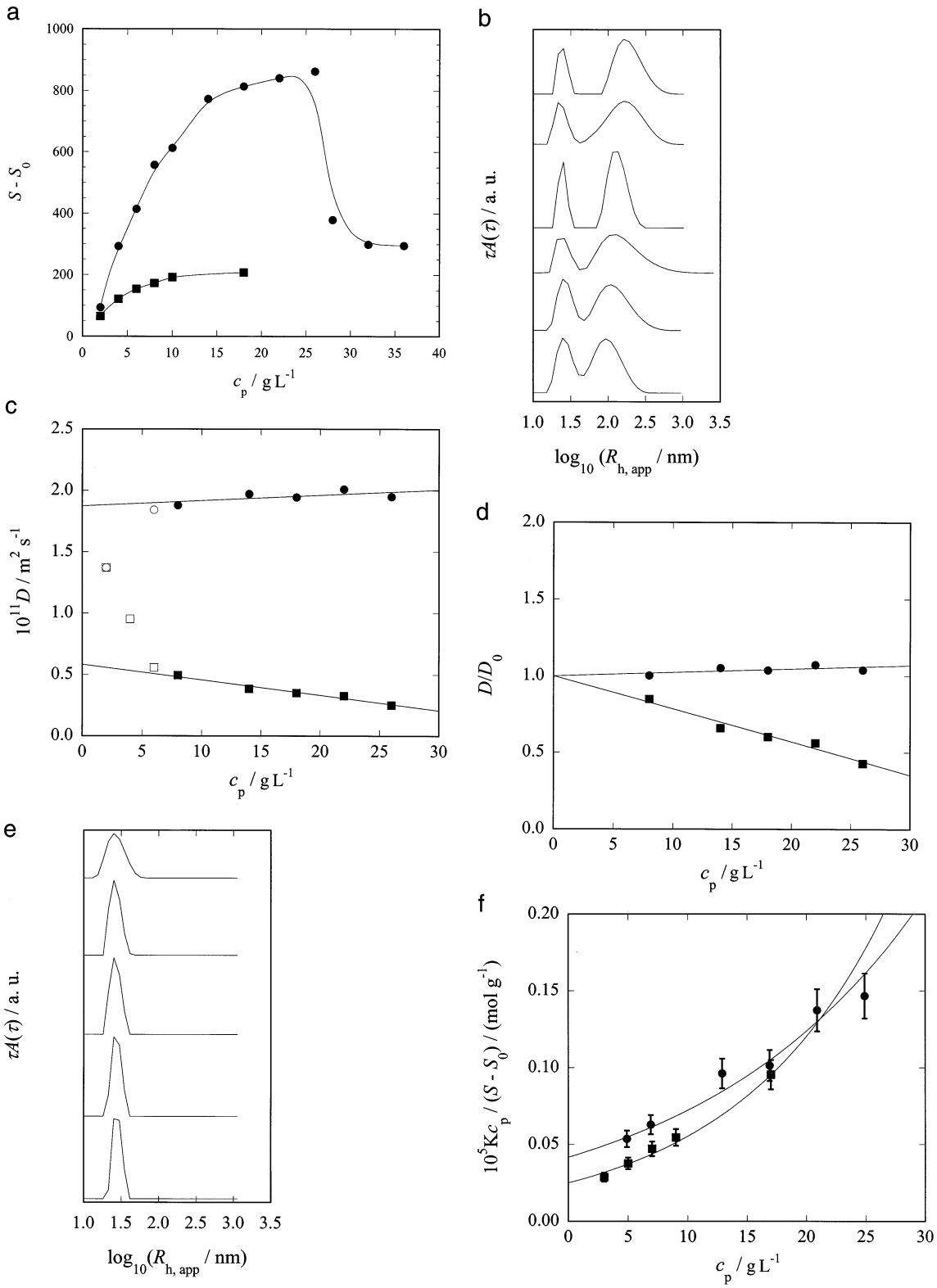

Figure 6. (a) Integrated excess intensity $S - S_0$ vs concentration of $P_{60}E_{348}$ + LC at $T = 50$ (●) and 60 °C (■). $T_s = 50$ °C. (b) Distributions of $R_{h,app}$ for $P_{60}E_{348}$ + LC at $T = T_s = 50$ °C. Concentrations of $P_{60}E_{348}$ (from the bottom): 6, 8, 14, 18, 22, and 26 g L^{-1}. (c) Concentration dependence of the translational diffusion coefficient, D, for micelles (●) and that of the apparent D for LC droplets (■). $T = T_s = 50$ °C. (Points not included in the linear regressions: micelles (○); LC droplets (□).) (d) Normalized, dimensionless parameter D/D_0 vs copolymer concentration. $T = T_s = 50$ °C. (e) Distributions of $R_{h,app}$ for $P_{60}E_{348}$ + LC at $T = 60$ °C and $T_s = 50$ °C. Concentrations of $P_{60}E_{348}$ (from the bottom): 4, 6, 8, 10, and 18 g L^{-1}. (f) Debye plots for $P_{60}E_{348}$ + LC at $T = 50$ (●) and 60 °C (■). $T_s = 50$ °C. Error bars: ±10%.

micelles. Unfortunately, this increase cannot be quantified in our present experiments.

Figure 6a shows $S - S_0$ vs c_p, at $T = 50$ and 60 °C, for $T_s = 50$ °C, following completion of solubilization. The interpretation is similar to that for Figure 5b, but the most conspicuous feature of this figure is that $S - S_0$ is larger at 50 °C than at 60 °C. The reason is that at 50 °C, there is partly unsolubilized LC in the system, leading to macroscopic phase separation. The LC

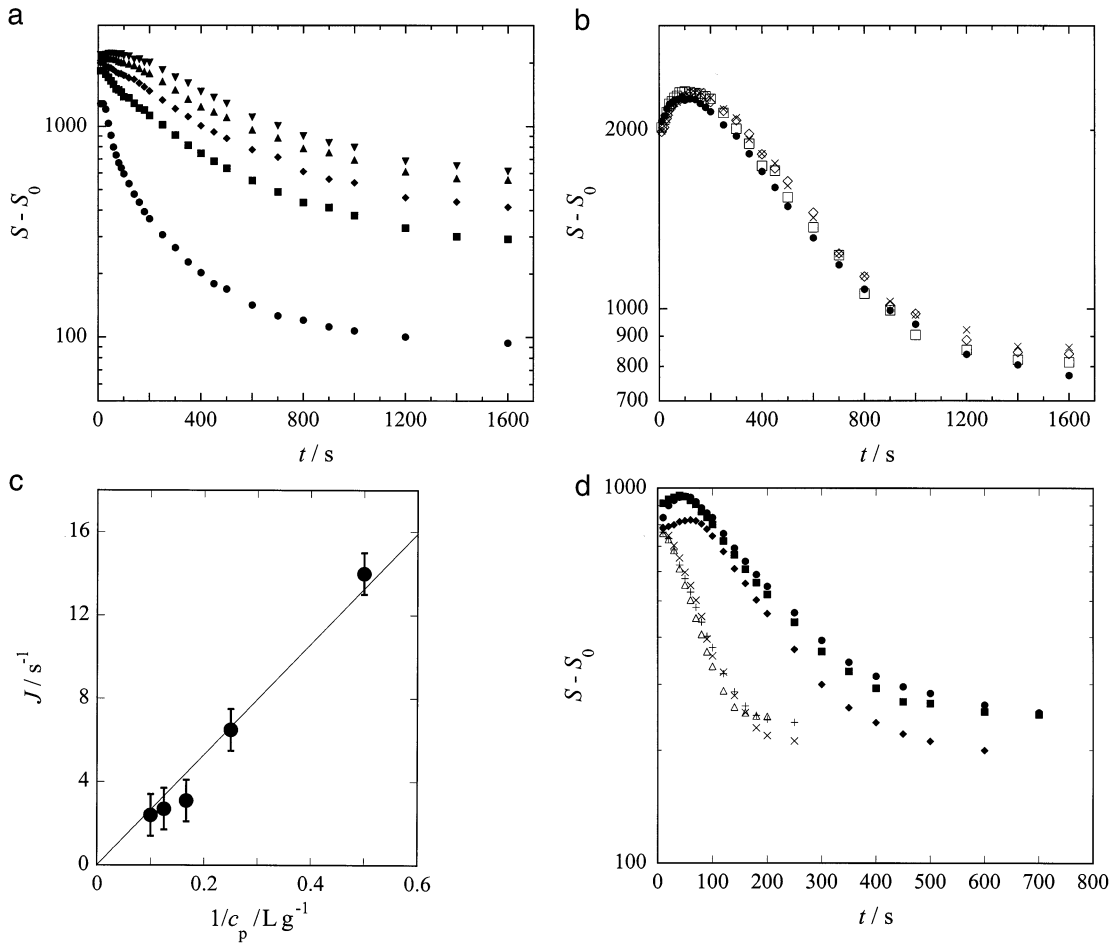

Figure 7. Integrated excess intensity $S - S_0$ as a function of solubilization time t, at $T = T_s = 50$ °C. Concentrations of $P_{60}E_{348}$: (a) 2 (●), 4 (■), 6 (◆), 8 (▲), and 10 g L^{-1} (▼); (b) 14 (●), 18 (□), 22 (◇), and 26 g L^{-1} (×). (c) Reciprocal concentration dependence of the solubilization rate J in dilute solutions. $T = T_s = 50$ °C. Error bars: ± 1 s^{-1}. (d) Integrated excess intensity $S - S_0$ at two different temperatures as a function of solubilization time t, for $T_s = 40$ °C. Concentrations of $P_{60}E_{348}$: 10 (●), 12 (■), and 26 g L^{-1} (◆) (T = 50 °C); 10 (×), 12 (+), and 26 g L^{-1} (△) (T = 60 °C).

droplets give a significant contribution to the total scattered intensity, which has to be taken into account. It has been noticed that the time-dependent autocorrelation functions possess a double-exponential decay rate when the experiments are carried out at a temperature equal to or smaller than the solubilization temperature (when $T \leq T_s$). The fast and slow relaxation rates reflect the dynamics of block copolymer micelles and aggregated LC, respectively. Thus, the distributions of apparent hydrodynamic radii are bimodal at $T \leq T_s$. Apparent hydrodynamic radii distributions are given in Figure 6b for $T = T_s = 50$ °C. The micelles have the smaller radius and the LC droplets/aggregates have the larger radius. The total intensity $S - S_0$ scattered by the micelles, which is inserted in the Debye equation, is calculated from the relative amplitudes of the peaks. It should be noted that despite the fact that the amplitude ratio of the slow-to-fast component where the slow and fast reflect LC droplets (d) and micelles (m), respectively (A_d/A_m), is relatively large, the corresponding mass concentration ratio (c_d/c_m) is relatively small. This is realized if the following rough estimation is made: The peak areas are directly proportional to the intensity, which in turn is proportional to the concentration and the molar mass of the solute. The intensities of the LC droplets (I_d) and the micelles (I_m) (the slow and the fast relaxation mode, respectively) are specified as

$$I_d \sim c_d M_d \qquad I_m \sim c_m M_m \tag{11}$$

Consider the following example. At 50 °C and $c_p = 22$ g L^{-1}, $I_s = 0.77$ and $I_f = 0.23$. The molecular weight of the micelles is $M_m \approx 2 \times 10^6$ g mol^{-1} (see Table 2) and that of the LC droplets, M_d, is approximately $(4/3)\pi R_h^3 N_A \rho$ so that using a density $\rho \approx 1 \times 10^6$ g m^{-3} and given that $R_h = 27 \times 10^{-9}$ m, $M_d = 50 \times 10^6$ g mol^{-1}. Accordingly, from eq 11:

$$c_d/c_m = (I_d/I_m)(M_m/M_d) \approx 0.13 \tag{12}$$

This calculation ignores the difference in refractive indices of the micelles and the LC droplets, which enters the calculation as

$$c_d/c_m = (I_d/I_m)(M_m/M_d)(\chi_m/\chi_d) \tag{13}$$

where χ denotes dn/dc. A reasonable estimate of $(\chi_m/\chi_d)^2 \approx 0.5$ implies that the slow component, which contributes 77% of the scattered light intensity, comprises only 7% (w/w) of the solute.

Figure 6c shows the corresponding concentration dependencies of the diffusion coefficients of micelles (fast) and LC droplets (slow). Only D values calculated at concentrations at which the two peaks in the DLS spectra are well separated have been used in the linear regressions in Figure 6c (filled symbols). As the concentration is decreased, there is a simultaneous deterioration of the peak resolution and eventually the bimodal distribution becomes unimodal (at $c_p = 2$ g L^{-1}), and this

behavior affects the characteristic relaxation times of the two components and, consequently, the diffusion coefficients (open circles). As expected, there is a negative concentration dependence of D_s. Considering eq 4, because $A_2 = N_A u/2M^2$ for spheres, where $u = 8\nu$ is the excluded volume, ν being the molecular volume, then A_2 is very small for the LC droplets ($M_d \approx 50 \times 10^6$ g mol^{-1}) and only the negative terms in eq 4 ($-k_f$ and $-2\nu_2$) contribute to k_D. This effect is clearly illustrated in Figure 6d where the normalized quantity D/D_0 is given as a function of c_p, and where the magnitude of the slope is equal to the thermodynamic virial coefficient k_D. Figure 6e shows the distributions of $R_{h,app}$ at $T = 60$ °C and $T_s = 50$ °C. Because $T > T_s$, only one peak is observed in each spectrum, attributed to micelles. The baselines of the correlation functions are overall very small (less than 5%), and the peak amplitudes are equal to those of the moments of the correlation function of the entire solution, indicating that there are no other scatterers than micelles in the system. In this case, the total excess intensity can be used directly $Kc_p/(S - S_0)$. Figure 6f shows the Debye plots at $T = 50$ and 60 °C, respectively, and for $T_s = 50$ °C. Similar to Figure 5a and published Debye functions of block copolymer micelles without LC, the concentration dependence of the quantity $Kc_p/(S - S_0)$ can be fit to a function based on the Percus−Yevick approximation. The term S has been multiplied with the fraction of the scattered intensity attributed to the micelles, which was calculated according to the discussion above involving eqs 11−13.

3.4. Solubilization Rate Measurements. Parts a and b of Figure 7 show $S - S_0$ as a function of solubilization time t in a semilogarithmic plot for various concentrations of $P_{60}E_{348}$, and with $T = T_s = 50$ °C. Samples were thermally equilibrated at 21 °C for 24 h whereafter the experiment was started, i.e., at $t_0 = 0$, $T = 21$ °C. After t_0 the temperature was increased rapidly to 50 °C by transferring the sample tube to a hot scattering cell. As mentioned above, there is a small maximum in $S - S_0$ present prior to the time at which the effect of solubilization is observed, which is a concentration dependent time, t'. The maximum is more distinct in Figure 7b. For all values of c_p, there is a decay in $S - S_0$ until a plateau value is reached at t'', the time at which c_s is attained. For polymer concentrations in the interval 2 g L^{-1} $\leq c_p \leq$ 26 g L^{-1}, $t'' \cong 1\,600$ s. However, the rate J depends on c_p. We have defined J as minus the magnitude of the initial slope in the plot of $S - S_0$ vs t, starting at t'. When c_p is increased from 2 to 10 g L^{-1} there is a continuous decrease in J, whereafter J attains a constant value of about 2.1 s^{-1} in the interval 10 g L^{-1} $\leq c_p \leq$ 26 g L^{-1}. The magnitude of the solubilization rate vs the reciprocal value of the copolymer concentration is depicted in Figure 7c. One may have guessed that J would be independent of c_p, because c_p and c_{LC} (the total concentration of LC integrated over all micelles) are directly proportional to each other (at saturation of block copolymer micelles with LC at T_s, the excess LC was removed by filtration, i.e., the ratio c_{LC}/c_p is constant), but apparently this is not the case. As the number of micelles per unit volume is increased, the solubilization rate decreases, and Figure 7c confirms inverse proportionality. A possible explanation is that the LC droplets are less stable at low copolymer concentrations, due to poorer surface stabilization, in which case the activity of the LC molecules at the LC−solution interface is high, consequently also in the solution, which will increase the diffusion rate into the micelles.

Figure 7d shows $S - S_0$ as a function of t for different concentrations of $P_{60}E_{348}$. In this experiment, initial solubilization was at 40 °C. Cooling to 21 °C precipitated the LC, which was then resolubilized at either 50 or 60 °C. This limited the amount of LC available to be solubilized at the higher temperatures and ensured that there was no unsolubilized LC left in the form of droplets at the end of the experiment. The final values of $S - S_0$ in Figure 7d compared to those in Figure 7b are consistent with this. As for the results in Figure 7b, the copolymer concentrations were relatively high ($c_p \geq 10$ g L^{-1}), reflected by the fact that J is independent of c_p, either at 50 °C ($J \cong 2.8$ s^{-1}) or at 60 °C ($J \cong 4.0$ s^{-1}). It is clear that an increase in temperature by 10 deg enhances the solubilization process significantly; for $c_p = 26$ g L^{-1}, $t'' \cong 700$ s at 50 °C, but only 200 s at 60 °C.

Acknowledgment. Dr. F. Heatley, Miss C. Chaibundit, and Mr. S. K. Nixon are gratefully acknowledged for help with the characterization of the block copolymer. The United Kingdom Engineering and Physical Sciences Research Council (EPSRC), grant GR/M51994, and The Royal Swedish Academy of Sciences are thanked for financial support.

References and Notes

(1) Chu, B. *Langmuir* **1995**, *11*, 414.
(2) Alexandridis, P.; Hatton, T. A. *Colloids Surf. A* **1995**, *96*, 1.
(3) Almgren, M.; Brown, W.; Hvidt, S. *Colloid Polym. Sci.* **1995**, *273*, 2.
(4) Chu, B.; Zhou, Z. K. In *Nonionic Surfactants*; Surfactant Science Series; Nace, V. M., Ed.; Marcel Dekker: New York, 1996; Vol. 60, p 67.
(5) Alexandridis, P. *Curr. Opin. Colloid Interface Sci.* **1997**, *2*, 478.
(6) Hamley, I. W. *The Physics of Block Copolymers*; Oxford University Press: Oxford, U.K., 1998.
(7) Gast, A. P. *Curr. Opin. Colloid Interface Sci.* **1997**, *2*, 258.
(8) Tuzar, Z.; Kratochvíl, P. In *Surface and Colloid Science*; Matijevic, E., Ed.; Plenum Press: New York, 1993; Vol. 15, p 1.
(9) Schillén, K.; Brown, W.; Coňák, Č. *Macromolecules* **1993**, *26*, 3611.
(10) Booth, C.; Attwood, D. *Macromol. Rapid Commun.* **2000**, *21*, 501.
(11) Iyama, K.; Nose, T. *Macromolecules* **1998**, *31*, 7356.
(12) Altinok, H.; Yu, G.-E.; Nixon, S. K.; Gorry, P. A.; Attwood, D.; Booth, C. *Langmuir* **1997**, *13*, 5837.
(13) Hamley, I. W.; Fairclough, J. P. A.; Ryan, A. J.; Ryu, C. Y.; Lodge, T. P.; Gleeson, A. J.; Pedersen, J. S. *Macromolecules* **1998**, *31*, 1188.
(14) Solans, C., Ed. *Industrial Applications of Microemulsions*; Surfactant Science Series; Marcel Dekker: New York, 1997; p 66.
(15) Evers, O. A.; Fleer, G. J.; Scheutjens, J. M. H. M.; Lyklema, J. *J. Colloid Interface Sci.* **1986**, *111*, 446.
(16) Erikson, L.; Alm, B. *Water Sci. Technol.* **1993**, *28*, 203.
(17) Müller, H.; Leube, W.; Tauer, K.; Förster, S.; Antonietti, M. *Macromolecules* **1997**, *30*, 2288.
(18) Juhasz, J.; Lenaerts, V.; Tan, P. V. M.; Ong, H. *J. Colloid Interface Sci.* **1990**, *136*, 168.
(19) Schmolka, I. R. *J. Biomed. Mater. Res.* **1972**, *6*, 571.
(20) Fendler, J. *Membrane Mimetic Chemistry*; Wiley: New York, 1983.
(21) Nagarajan, R.; Ganesh, K. *J. Chem. Phys.* **1993**, *98*, 7440.
(22) Hurter, P. N.; Hatton, T. A. *Langmuir* **1992**, *8*, 1291.
(23) Kiserow, D.; Prochazka, K.; Ramireddy, C.; Tuzar, Z.; Munk, P.; Webber, S. E. *Macromolecules* **1992**, *25*, 461.
(24) Evans, D. F.; Wennerström, H. *The Colloidal Domain: where physics, chemistry, biology and technology meet*, 2nd ed.; Wiley-VCH: New York, 1999; p 204.
(25) Gadelle, F.; Koros, W. J.; Schechter, R. S. *Macromolecules* **1995**, *28*, 4883.
(26) Yang, Z.; Pousia, E.; Heatley, F.; Price, C.; Booth, C.; Castelletto, V.; Hamley, I. W. *Langmuir* **2001**, *17*, 2106.
(27) Iannacchione, G. S.; Crawford, G. P.; Qian, S.; Doane, J. W.; Finotello, D. *Phys. Rev. E* **1996**, *53*, 2402.
(28) Crawford, G. P.; Stannarius, R.; Doane, J. W. *Phys. Rev. A* **1991**, *44*, 2558.
(29) Widawski, G.; Rawiso, M.; François, B. *Nature* **1994**, *369*, 387.
(30) Altinok, H.; Nixon, S. K.; Gorry, P. A.; Attwood, D.; Booth, C.; Kelarakis, A.; Havredaki, V. *Colloids Surf. B* **1999**, *16*, 73.
(31) Heatley, F.; Luo, Y.-Z.; Ding, J.-F.; Mobbs, R. H.; Booth, C. *Macromolecules* **1988**, *21*, 2713.
(32) Yu, G.-E.; Masters, A. J.; Heatley, F.; Booth, C.; Blease, T. G. *Macromol. Chem. Phys.* **1994**, *195*, 1517.
(33) Deng, N.-J.; Luo, Y.-Z.; Tanodekaew, S.; Bingham, N.; Attwood, D.; Booth, C. *J. Polym. Sci., Part B: Polym. Phys.* **1995**, *33*, 1085.

(34) Nicolai, T.; Brown, W.; Johnsen, R. M.; Štěpánek, P. *Macromolecules* **1990**, *23*, 1165.
(35) Provencher, S. W. *Makromol. Chem.* **1979**, *180*, 201.
(36) Vink, H. *J. Chem. Soc., Faraday Trans. 1* **1985**, *81*, 1725.
(37) Yang, Z.; Kelarakis, A.; Pousia, E.; Nixon, S. K.; Price, C.; Booth, C.; Hamley, I. W.; Castelletto, V.; Fundin, J. *Langmuir* **2001**, *17*, 8085.
(38) Zhou, Z.; Chu, B. *J. Colloid Interface Sci.* **1988**, *126*, 171.
(39) Attwood, D.; Collett, J. H.; Tait, C. J. *Int. J. Pharm.* **1985**, *26*, 25.
(40) Nagarajan, R. *Colloids Surf. B: Biointerfaces* **1999**, *16*, 55.
(41) Fundin, J.; Castelletto, V.; Yang, Z.; Hamley, I. W.; Waigh, T. A.; Price, C. Submitted to *Colloid Polym. Sci*.
(42) Vrij, A. *J. Chem. Phys.* **1978**, *69*, 1742.
(43) Carnahan, N. F.; Starling, K. E. *J. Chem. Phys.* **1969**, *51*, 635.
(44) Mai, S.-M.; Booth, C.; Nace, M. *Eur. Polym. J.* **1997**, *33*, 991.